# Eigenfrequency loci crossings, veerings and mode splittings of two cantilevers coupled by an overhang

Journal of Physics Communications

OPEN ACCESS

REVISED
26 July 2020

ACCEPTED FOR PUBLICATION
31 July 2020

PUBLISHED
12 August 2020



PAPER

# Eigenfrequency loci crossings, veerings and mode splittings of two cantilevers coupled by an overhang

**Yin Zhang**[1,2], **Yuri Petrov**[3,4] **and Ya-Pu Zhao**[1,2]

[1] State Key Laboratory of Nonlinear Mechanics (LNM), Institute of Mechanics, Chinese Academy of Sciences, Beijing 100190, People's Republic of China
[2] School of Engineering Science, University of Chinese Academy of Sciences, Beijing 100049, People's Republic of China
[3] St-Petersburg State University, St-Petersburg, 198504, Russia
[4] Institute of Problems of Mechanical Engineering, St-Petersburg, 199178, Russia

**E-mail:** zhangyin@lnm.imech.ac.cn

**Keywords:** eigenfrequency, crossing, veering, mode splitting

## Abstract

Eigenfrequency loci veering, which indicates strong mode coupling and sometimes mode localization, is a much sought-after property in the applications of mass sensing and opto/electromechanics. A weak physical coupling is the mechanism responsible for the eigenfrequency loci veering and overhang is a widely used structure to realize such mechanism. A continuum model, which is more accurate and straightforward as compared with the discrete models, is presented for the structure of two overhanged cantilevers. The eigenvalue problem formulation based on this continuum model leads to a direct computation of the eigenfrequencies, which does not involve any numerical discretization procedure. A comprehensive study on the eigenfrequency loci veerings and mode splittings of the overhanged structure is presented. The influences of various parameters on the eigenfrequency loci crossing and veerings are also systematically studied. An efficient optimum design tool for the eigenfrequency loci veering of an overhanged structure is provided by the continuum model together with a direct computation method.

## 1. Introduction

In 1958, Anderson proposed a model of electron transport predicating the phenomenon of 'absence of diffusion' [1], which now is known as Anderson localization in solid-state physics and variously called energy confinement or mode localization in structural mechanics [2]. The theory of Anderson localization essentially says that the conventional transport as predicated by the Boltzmann or diffusion equation breaks down in disordered systems. In an 'ordered' solid, once the disorder is introduced by imperfections or impurities, the eigenmodes of the Schrödinger equation governing the electron motions may become localized rather than keeping extended, the metallic conduction would be impossible [3]. Therefore, the solid may abruptly change from a metallic conductor to a semiconductor or an insulator. Anderson's work on the localization theory is the corner stone for his award of the Nobel Prize for physics in 1977 [4]. The phenomenon of mode localization is also frequently encountered in various periodic structures, such as large space structures with cyclic symmetry (e.g. communication antennas and solar energy collectors) [3], turbomachinery rotor (with mistuned blades) [5], coupled pendula [6, 7], multi-spanned string [2] and beams [8, 9], etc. In a linear vibration, an eigenmode or mode is an eigenvector and an eigenfrequency is an eigenvalue. The mode localization is closely related with another phenomenon called the eigenvalue loci veering in many problems of solid state physics and structural mechanics. According to Pierre [7], 'strong mode localization and eigenvalue loci veering are two manifestations of the same drastic phenomenon occurring in disordered systems'. When the mistuning/disorder parameters vary, two of the eigenvalues, which physically can represent the resonance frequencies [2, 6–8] or the buckling loads [9], may rapidly approach each other and then diverge abruptly without crossing. This rapid approaching-diverging behavior is called veering in structural mechanics [10, 11], which is more straightforwardly called

avoided crossing [12, 13] or anti-crossing [14] in solid-state physics. Both the mode localization and eigenvalue loci veering are a catastrophic phenomenon [7], i.e., a small variation in the mistuning parameters results in the large variations of eigenvalues and mode shapes. The mode localization or energy confinement as suggested by their names indicates the motion/energy is confined in (small) geometric regions, which is harmful to the life span and integrity of a structure [3, 5]. While, when its catastrophic nature is ingeniously exploited, the eigenvalue loci veering can be very useful in the applications of mass sensing [15–22] and cavity opto/electromechanics [23–32].

Coupling is the mechanism responsible for the veering behavior of a disordered system [10, 11]. A discrete system consisting of $N$ identical subsystems is a $N$-fold degeneracy system if the subsystems are uncoupled. Coupling, however small, changes the system uncoupled state to collective oscillations [6]. Although coupling does not necessarily prevent a crossing, coupling can provide a degeneracy-splitting mechanism that forbids any two of the coupled system eigenfrequencies to be the same (i.e., crossing) and thus leads to the veering [6]. When the degeneracy is splitted by a disorder, the strong mode localization occurs because the weak coupling between the subsystems cannot produce the extended modes in which all subsystems contribute more or less the same amplitude [6]. In mass resonator sensors, the coupling can be realized by an overhang connecting several substructures [15, 16, 19, 20] or by applying an electrostatic force [21, 22] or by both overhang and electrostatic force [17, 18]. In optomechanics, a mechanical resonator forms an end of the Fabry-Pérot (FP) optical cavity. The radiation or bolometric pressure induced by the optical cavity is the driving force for the mechanical resonator to vibrate, which in turn changes the optical path length and affects the photon density stored in the FP cavity [30, 32, 33]. As a result, the optical resonance frequency is shifted and therefore, the optomechanical coupling is realized, which is also viewed as the entanglement between photon and phonon [13]. The optomechanical coupling results in a velocity-dependent force acting on the mechanical resonator, which can be either damping or anti-damping [32]. The damping effect is utilized to cool a macroscopic mechanical resonator [33], i.e., to reduce its thermal motion, and the quantum ground state has been achieved [24]. On the other hand, the anti-damping effect is used to amplify the resonator motion and realize the self-oscillation [30]. One development of optomechanics is to replace the optical cavity by an electrical one [23, 28], which provides more convenient and versatile manipulations in the nanoelectromechanical systems (NEMS) [28] and optomechanics thus becomes electromechanics. Another drastic development is no optical/electrical cavity at all, which is replaced by ahigher mode of the mechanical resonator [13, 25–27, 29]. Mahboob *et al* [25] and Okamoto *et al* [26] realized the coupling by connecting two resonator beams via overhangs. Faust's is to couple the in-plane and out-of-plane modes of one resonator string by applying electrostatic force [27, 29]. Similarly, Mathew's is to couple the flexural modes of a circular membrane by applying electrostatic force [13].

Due to its catastrophic nature, a tiny introduction of disorder, such as adsorption of an analyte, can cause rather significant variations of the eigenfrequencies and mode shapes of a coupled structure, which is the sensing mechanism of many mass resonators [15, 16, 20, 34]. In an overhanged mass resonator based on the mode shape sensing mechanism, the effect of mode localization needs to be enhanced to increase its sensitivity [15, 16, 35]. The enhancement mechanism is to reduce the coupling stiffness [15, 20]. For the resonator with two overhanged cantilevers, the physical coupling stiffness $k_c$ and the cantilever effective stiffness $k$ are with the following relation [20]

$$\frac{k_c}{k} = \frac{\omega_2^2 - \omega_1^2}{2\omega_1^2}, \tag{1}$$

where $\omega_2$ and $\omega_1$ are the two (measured) adjacent eigenfrequencies and $\omega_2 > \omega_1$. The difference between two eigenfrequencies ($\omega_2 - \omega_1$) is termed the frequency splitting [14]. Clearly, according to the above equation, the smallest frequency splitting results in the smallest $k_c$ for a given $k$. This smallest frequency splitting is also called veering neck [21] or veering width [35]. The eigenvalue loci veering is related to the closely spaced eigenfrequencies [36] and the closeness of the eigenfrequency spacing can be used to evaluate the degree of mode coupling [37]. Veering signifies strong mode coupling [14], which becomes stronger as its veering neck becomes smaller [37]. An essential information conveyed by equation (1) is that a weak physical coupling ($k_c$) results in an eigenfrequency loci veering, which corresponds to a strong mode coupling. Clearly, in equation (1) the physical coupling is also indicated by the frequency splitting. An effective strategy to seek the strong mode coupling, or say, to achieve a weak physical coupling is to design or tune a structure with closely spaced eigenfrequencies. For example, Shkarin *et al* [31] used two modes of a square membrane with the eigenfrequency difference of 0.07% to achieve a nearly complete (99.5%) hybridization of optical and mechanical modes. Okamoto *et al* [26] used the two modes of the overhanged beams with the closely spaced eigenfrequencies of 293.94 kHz and 294.37 kHz to achieve a high efficient energy transfer between two modes. Compared with the quantized two-ion oscillators which are strongly coupled by the Coulomb interaction potential [12], a known technical difficulty in the opto/electromechanics is to achieve the performance of the long-lived collective motions of a macroscopically large mechanical resonator due to the lack of strong opto/electromechanical mode coupling [23]. Therefore, in order

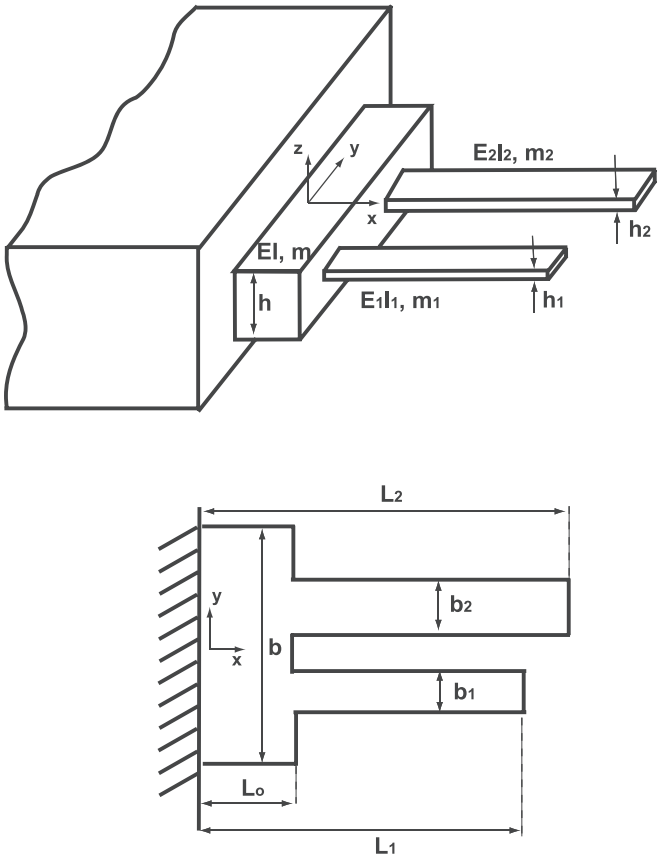


**Figure 1.** The schematic diagrams of an overhanged cantilever structure with two beams and their dimensions.

to achieve the strongest mode coupling, a major effort in the opto/electromechanics and related researches is to design or tune the control parameters to identify the veering locus/loci [12, 13, 23, 25–29, 31, 32].

As shown in figure 1, an overhang, which is variously called a shared mechanical ledge [38] or shuttle mass [17, 18], connects two cantilevers. Overhang provides a simple and direct coupling mechanism for (sub) structures, which has been used in various applications [15–20, 25, 26, 38]. The discrete models with the lumped parameters have been used to study the overhanged structure [15, 17, 19, 20, 25, 26, 38, 39]. In this study, we provide a continuum mechanics model to study the two overhanged cantilevers. The discrete model suffers from the following two major drawbacks, which are addressed one by one by our continuum model. One is how to obtain those lumped parameters. For a discrete model to start, the lumped parameters must be given. For example, the effective overhanged cantilever stiffness of $k$ is found by a continuum mechanics approach [40] and then the effective coupling stiffness of $k_c$ in equation (1) is actually obtained by measuring two adjacent resonance frequencies of $\omega_1$ and $\omega_2$ [20]. Finding $k$ and $k_c$ is not an easy task [40]. A further problem is that $k_c$ and $k$ are different for different modes [40]. A general approach is to use the experimentally measured resonance frequencies to find those lumped parameters by solving an inverse problem [41], which is complex and difficult. In comparison, there is no such need to specify those parameters in our continuum model. The other drawback is that in those discrete models [15, 17, 19, 20, 25, 26, 38], only two adjacent modes are selected mainly due to the difficulty of specifying the lumped parameters. This can cause three major problems. Firstly, there is only one coupling/mixing/interaction between two modes in a discrete model. For a continuum structure, there are infinite modes. The influence of the $\omega_2 - \omega_3$ mode coupling on the $\omega_2$ mode sometimes can even be larger than that of the $\omega_2 - \omega_1$ mode coupling. Together with the error of specifying the lumped parameters, this one-interaction only discrete model shows rather significantly different results from those of experiments [19]. In our continuum model, all mode interactions are included and thus more accurate results are expected. Secondly, as only two modes are included in a discrete model, the focus has to be on these two modes only. In the mode-shape based mass sensing mechanism [15, 16, 35], weak physical coupling, or say, veering, is preferred. In contrast, in the eigenfrequency-shift based mass sensing mechanism, strong physical coupling, which is indicated by large separations between eigenfrequencies, is preferred [39].

Through the continuum model, we provide a comprehensive view on the mode interactions by presenting the eigenfrequency spectra, in which veerings and mode splittings can be easily identified. A pattern is found in

this study: a veering locus of two adjacent eigenfrequencies is also the locus of the largest separation of two different adjacent eigenfrequencies. The finding of this pattern may help a mass resonator to switch easily from the mode-shape based mechanism to the eigenfrequency-shift based mechanism and vice versa. Unlike the electrostatic coupling mechanism [13, 21, 22, 27, 29], which can be easily optimized during an experiment by tuning the DC gate voltage, once an overhang is fabricated, it is a fixed structure. There is a huge demand for optimizing the overhanged structure [15], which brings up the third problem: As the discrete model only handles two modes each time and the difficulty of specifying lumped parameters, it will be extremely difficult and complex to use the discrete model as an optimization design tool. Very few attempts at optimizing the coupled cantilevers by an overhang are tried. One example is the experimental approach on two identical overhanged cantilevers, in which the only optimizing parameter is the separation distance between two cantilevers [20]. Our continuum model presents a systematic and comprehensive study on the impacts of various parameters on the eigenfrequencies. For example, the geometric parameters, such as the length, width and thickness (which implicitly includes the separation distance) and material property (Young's modulus) of an overhang together with the various differences such as mass, stiffness and length between two cantilevers. The previous discrete models [15, 17, 19, 20, 25, 26, 38, 39] in essence only offer some qualitative explanations on the experimental findings rather than providing an optimization tool. With this continuum model, an efficient and more accurate optimization tool is presented.

## 2. Model development

In the schematic diagram of an overhanged cantilever structure in figure 1, one end of the overhang sis connected with two beams and the other is clamped. Here $b$, $h$ and $L_o$ are the width, thickness and length of the overhang, respectively. The corresponding parameters for beam 1 and 2 are $b_1$, $h_1$ $L_1$ and $b_2$, $h_2$ $L_2$. The system kinetic energy ($T$), which consists of three parts: Overhang and two beams, is given as follows

$$T = \int_0^{L_o} \frac{m}{2}\left(\frac{\partial w}{\partial t}\right)^2 dx + \int_{L_o}^{L_1} \frac{m_1}{2}\left(\frac{\partial w_1}{\partial t}\right)^2 dx + \int_{L_o}^{L_2} \frac{m_2}{2}\left(\frac{\partial w_2}{\partial t}\right)^2 dx. \tag{2}$$

Here $m$, $m_1$ and $m_2$ are the mass per unit length of the overhang, beam 1 and beam 2, respectively. For the rectangular sections, $m = \rho bt$, $m_1 = \rho_1 b_1 t_1$ and $m_2 = \rho_2 b_2 t_2$ ($\rho$, $\rho_1$ and $\rho_2$ are the densities of the overhang and the two beams, respectively). The three transverse displacements of $w$, $w_1$ and $w_2$ are defined as the following:

$$\begin{cases} w, & 0 \leqslant x \leqslant L_o \quad \text{(Displacement of the overhang)} \\ w_1, & L_o \leqslant x \leqslant L_1 \quad \text{(Displacement of beam 1)} \\ w_2, & L_o \leqslant x \leqslant L_2 \quad \text{(Displacement of beam 2).} \end{cases} \tag{3}$$

The system potential/bending energy ($V$) is given as follows

$$V = \int_0^{L_o} \frac{EI}{2}\left(\frac{\partial^2 w}{\partial x^2}\right)^2 dx + \int_{L_o}^{L_1} \frac{E_1 I_1}{2}\left(\frac{\partial^2 w_1}{\partial x^2}\right)^2 dx + \int_{L_o}^{L_2} \frac{E_2 I_2}{2}\left(\frac{\partial^2 w_2}{\partial x^2}\right)^2 dx, \tag{4}$$

where $E$, $E_1$, $E_2$ and $I$, $I_1$, $I_2$ are the Young's moduli and the second moments of area of the overhang and two beams, respectively. For rectangular cross sections, $I = bh^3/12$, $I_1 = b_1 h_1^3/12$ and $I_2 = b_2 h_2^3/12$, respectively. By applying the Hamilton's Principle, i.e., $\delta \int_{t_1}^{t_2} (T - V)\, dt = 0$, the following governing equations are derived:

$$\begin{cases} m\frac{\partial^2 w}{\partial t^2} + EI\frac{\partial^4 w}{\partial x^4} = 0, & 0 \leqslant x \leqslant L_o \\ m_1\frac{\partial^2 w_1}{\partial t^2} + E_1 I_1\frac{\partial^4 w_1}{\partial x^4} = 0, & L_o \leqslant x \leqslant L_1 \\ m_2\frac{\partial^2 w_2}{\partial t^2} + E_2 I_2\frac{\partial^4 w_2}{\partial x^4} = 0, & L_o \leqslant x \leqslant L_2. \end{cases} \tag{5}$$

The corresponding twelve boundary conditions are also derived from the Hamilton's Principle as follows:

$$\begin{aligned} &w(0) = 0, \quad \frac{\partial w}{\partial x}(0) = 0, \quad \frac{\partial^2 w_1}{\partial x^2}(L_1) = 0, \quad \frac{\partial^3 w_1}{\partial x^3}(L_1) = 0, \quad \frac{\partial^2 w_2}{\partial x^2}(L_2) = 0, \quad \frac{\partial^3 w_2}{\partial x^3}(L_2) = 0, \\ &w(L_o) = w_1(L_o), \quad \frac{\partial w}{\partial x}(L_o) = \frac{\partial w_1}{\partial x}(L_o), \quad w(L_o) = w_2(L_o), \quad \frac{\partial w}{\partial x}(L_o) = \frac{\partial w_2}{\partial x}(L_o), \\ &EI\frac{\partial^2 w}{\partial x^2}(L_o) = E_1 I_1\frac{\partial^2 w_1}{\partial x^2}(L_o) + E_2 I_2\frac{\partial^2 w_2}{\partial x^2}(L_o), \quad EI\frac{\partial^3 w}{\partial x^3}(L_o) = E_1 I_1\frac{\partial^3 w_1}{\partial x^3}(L_o) + E_2 I_2\frac{\partial^3 w_2}{\partial x^3}(L_o). \end{aligned} \tag{6}$$

The first six equations are the cantilevered boundary conditions; the last six equations are to ensue the continuity of displacement, slope, moment and shear force at $x = L_o$ [42]. Here the Euler-Bernoulli beam model, which is indicated by the expressions of the kinetic and potential energies, is used. The two beams are coupled via the governing equations and the boundary conditions. Physically, the overhang is the part shared by the two beams,

in which the two beams are with the same transverse displacement of $w$ and two beams are thus coupled. The continuity conditions of the last six equations of equation (6) also enforce the coupling from the boundary condition angle. There is an issue on the beam model here: when $L_o$ is small, the overhang part geometrically is a plate rather than a beam. While, when a plate bends into a cylindrical surface, it is still essentially a one-dimensional structure and therefore, the beam model applies [43, 44]. Our overhang (plate) here is in the same geometric configuration as that of Whitney's plate, in which the beam model is used [44]. Besides the issue of the plate behavior, the overhang portion is rather chunky when $L_o$ is small. In such scenario, the Timoshenko model of a thick beam instead of the Euler-Bernoulli model of a slender beam should be adopted. Due to the consideration of the rotary inertia and the shear force, all the eigenfrequencies computed by the Timoshenko beam model are smaller than those by the Euler-Bernoulli model [45]. This can more or less affects the accuracy of the eigenfrequency computation of an overhanged structure.

The following dimensionless quantities are introduced [46]:

$$\tau = \sqrt{\frac{E_1 I_1}{m_1 L_1^4}}\, t, \quad \xi = \frac{x}{L_1}, \quad \xi_o = \frac{L_o}{L_1}, \quad \xi_2 = \frac{L_2}{L_1}, \quad W = \frac{w}{L_1}, \quad W_1 = \frac{w_1}{L_1}, \quad W_2 = \frac{w_2}{L_1}. \tag{7}$$

The governing equations of equation (5) are now non-dimensionalized as the following:

$$\begin{cases} \alpha \frac{\partial^2 W}{\partial \tau^2} + \gamma \frac{\partial^4 W}{\partial \xi^4} = 0, & 0 \leqslant \xi \leqslant \xi_o \\ \frac{\partial^2 W_1}{\partial \tau^2} + \frac{\partial^4 W_1}{\partial \xi^4} = 0, & \xi_o \leqslant \xi \leqslant 1 \\ (1+\Delta_1)\frac{\partial^2 W_2}{\partial \tau^2} + (1+\Delta_2)\frac{\partial^4 W_2}{\partial \xi^4} = 0, & \xi_o \leqslant \xi \leqslant \xi_2. \end{cases} \tag{8}$$

The dimensionless quantities in equation (8) are defined as follows:

$$\alpha = \frac{m}{m_1} = \frac{\rho b h}{\rho_1 b_1 h_1}, \quad \gamma = \frac{EI}{E_1 I_1} = \frac{E b h^3}{E_1 b_1 h_1^3}, \quad \Delta_1 = \frac{m_2}{m_1} - 1 = \frac{\rho_2 b_2 h_2}{\rho_1 b_1 h_1} - 1,$$
$$\Delta_2 = \frac{E_2 I_2}{E_1 I_1} - 1 = \frac{E_2 b_2 h_2^3}{E_1 b_1 h_1^3} - 1. \tag{9}$$

Physically, $\alpha$ and $\gamma$ are the dimensionless mass per unit length and bending stiffness of the overhang; $\Delta_1$ and $\Delta_2$ are the beam 2 dimensionless deviations of the mass per unit length and bending stiffness from those of beam 1, respectively. By assuming $W = U(\xi)e^{i\omega\tau}$, $W_1 = U_1(\xi)e^{i\omega\tau}$, $W_2 = U_2(\xi)e^{i\omega\tau}$ ($\omega$: the dimensionless circular frequency) and substituting them into equation (8), the following solution forms are obtained

$$\begin{cases} U(\xi) = A_1 \sin(\kappa\beta\xi) + A_2 \cos(\kappa\beta\xi) + A_3 \sinh(\kappa\beta\xi) + A_4 \cosh(\kappa\beta\xi), & 0 \leqslant \xi \leqslant \xi_o \\ U_1(\xi) = B_1 \sin(\beta\xi) + B_2 \cos(\beta\xi) + B_3 \sinh(\beta\xi) + B_4 \cosh(\beta\xi), & \xi_o \leqslant \xi \leqslant 1 \\ U_2(\xi) = C_1 \sin(\kappa_2\beta\xi) + C_2 \cos(\kappa_2\beta\xi) + C_3 \sinh(\kappa_2\beta\xi) + C_4 \cosh(\kappa_2\beta\xi), & \xi_o \leqslant \xi \leqslant \xi_2. \end{cases} \tag{10}$$

Where $A_i$, $B_i$ and $C_i$ ($i = 1$ to 4) are the twelve unknown constants to be determined. The dimensionless quantities of $\beta$, $\kappa$ and $\kappa_2$ are defined as the following:

$$\beta = \sqrt{\omega}, \quad \kappa = \sqrt[4]{\frac{\alpha}{\gamma}}, \quad \kappa_2 = \sqrt[4]{\frac{1+\Delta_1}{1+\Delta_2}}. \tag{11}$$

The boundary conditions of equation (6) now become the dimensionless ones as follows:

$$U(0) = 0, \quad \frac{\partial U}{\partial \xi}(0) = 0, \quad \frac{\partial^2 U_1}{\partial \xi^2}(1) = 0, \quad \frac{\partial^3 U_1}{\partial \xi^3}(1) = 0, \quad \frac{\partial^2 U2}{\partial \xi^2}(\xi_2) = 0, \quad \frac{\partial^3 U_2}{\partial \xi^3}(\xi_2) = 0,$$
$$U(\xi_o) = U_1(\xi_o), \quad \frac{\partial U}{\partial \xi}(\xi_o) = \frac{\partial U_1}{\partial \xi}(\xi_o), \quad U(\xi_o) = U_2(\xi_o), \quad \frac{\partial U}{\partial \xi}(\xi_o) = \frac{\partial U_2}{\partial \xi}(\xi_o),$$
$$\gamma \frac{\partial^2 U}{\partial \xi^2}(\xi_o) = \frac{\partial^2 U_1}{\partial \xi^2}(\xi_o) + (1+\Delta_2)\frac{\partial^2 U_2}{\partial x^2}(\xi_o), \quad \gamma \frac{\partial^3 U}{\partial \xi^3}(\xi_o) = \frac{\partial^3 U_1}{\partial \xi^3}(\xi_o) + (1+\Delta_2)\frac{\partial^3 U_2}{\partial x^3}(\xi_o). \tag{12}$$

In conjunction with equations (10) and (12), an eigenvalue problem can formulated by setting the determinant of a 12 × 12 matrix zero. However, significant computation effort can be saved by using the cantilevered boundary conditions. By substituting equation (10) into the first six boundary conditions of equation (12), the following solution forms are obtained

$$\begin{cases} U = A_1[\sin(\kappa\beta\xi) - \sinh(\kappa\beta\xi)] + A_2[\cos(\kappa\beta\xi) - \cosh(\kappa\beta\xi)], & 0 \leqslant \xi \leqslant \xi_o \\ U_1 = B_1[\sin(\beta\xi) + b_{31}\sinh(\beta\xi) + b_{41}\cosh(\beta\xi)] + B_2[\cos(\beta\xi) + b_{32}\sinh(\beta\xi) + b_{42}\cosh(\beta\xi)], & \xi_o \leqslant \xi \leqslant 1 \\ U_2 = C_1[\sin(\kappa_2\beta\xi) + c_{31}\sinh(\kappa_2\beta\xi) + c_{41}\cosh(\kappa_2\beta\xi)] + C_2[\cos(\kappa_2\beta\xi) + c_{32}\sinh(\kappa_2\beta\xi) + c_{42}\cosh(\kappa_2\beta\xi)], & \xi_o \leqslant \xi \leqslant \xi_2, \end{cases} \tag{13}$$

where $b_{31}, b_{32}, b_{41}, b_{42}$ and $c_{31}, c_{32}, c_{41}, c_{42}$ are the eight constants defined in appendix. Now by substituting equation (13) into the last six boundary conditions of equation (12), the following equation is found:

$$\mathbf{K}\vec{\mathbf{V}} = \begin{pmatrix} k_{11} & k_{12} & k_{13} & k_{14} & 0 & 0 \\ k_{21} & k_{22} & k_{23} & k_{24} & 0 & 0 \\ k_{31} & k_{32} & 0 & 0 & k_{35} & k_{36} \\ k_{41} & k_{42} & 0 & 0 & k_{45} & k_{46} \\ k_{51} & k_{52} & k_{53} & k_{54} & k_{55} & k_{56} \\ k_{61} & k_{62} & k_{63} & k_{64} & k_{65} & k_{66} \end{pmatrix} \begin{pmatrix} A_1 \\ A_2 \\ B_1 \\ B_2 \\ C_1 \\ C_2 \end{pmatrix} = \begin{pmatrix} 0 \\ 0 \\ 0 \\ 0 \\ 0 \\ 0 \end{pmatrix} \tag{14}$$

Here $\vec{\mathbf{V}}$ is a vector defined as $\vec{\mathbf{V}}^T = (A_1, A_1, B_1, B_2, C_1, C_2)$; $\mathbf{K} = \mathbf{K}(\beta)$ is a $6 \times 6$ matrix and its elements are given in appendix. By setting the determinant of $\mathbf{K}$ zero, an eigenvalue problem is formulated and the system eigenfrequencies can thus be obtained numerically by the Newton-Raphson method [47]. When an eigenfrequency is found and substituted into the above equation, the following equation is obtained by setting $C_2 = 1$.

$$\begin{pmatrix} k_{11} & k_{12} & k_{13} & k_{14} & 0 \\ k_{21} & k_{22} & k_{23} & k_{24} & 0 \\ k_{31} & k_{32} & 0 & 0 & k_{35} \\ k_{41} & k_{42} & 0 & 0 & k_{45} \\ k_{51} & k_{52} & k_{53} & k_{54} & k_{55} \end{pmatrix} \begin{pmatrix} A_1 \\ A_2 \\ B_1 \\ B_2 \\ C_1 \end{pmatrix} = \begin{pmatrix} 0 \\ 0 \\ -k_{36} \\ -k_{46} \\ -k_{56} \end{pmatrix} \tag{15}$$

Once an eigenfrequency is substituted into the above equation, the constants of $A_1, A_2, B_1, B_2$ and $C_1$ can be easily found by equation (15). With the substitution of these constants and $C_2 = 1$ into equation (13), the corresponding eigenvector is obtained.

Here we need to emphasize that equation (14) is analytically derived and the eigenfrequency computation is a direct one, which does not involve any numerical discretization procedure. As in the crossing or veering regions, the two eigenfrequencies are very close. As a result, some numerical discretization methods can lead to a wrong conclusion on whether the eigenvalues cross or veer even though their computational errors are extremely small [10]. Mathematically, the reason is that those discretization methods cannot preserve the self-adjointness property of a continuous system [11], which introduces wrongful and unphysical coupling [10]. A vivid example is given by Leissa [10] that the analytical results show the eigenfrequencies of the 3-1 and 1-3 modes of a square membrane cross each other; while, a numerical discretization method shows the wrong computational result of veering. The recent developments [48–51] in computational mechanics using the artificial neural network (ANN) algorithm may overcome this discretization-induced problem. In the ANN algorithm, solving a partial differential equation (PDE), such as the governing equation of equation (8), is formulated as an optimization problem, in which the variational energy [48] or the user-defined loss function [49–51] is minimized. The essence of an ANN algorithm is iteration [48, 49] and the PDE governing equations serve as the guidance to tell how to search the next points of realizing the minimization [49]. As the ANN algorithm is mesh-free [50], the aforementioned discretization-induced problem by the classical numerical methods such as finite element and finite difference may thus be avoided.

## 3. Results and discussion

The above derivations are a general one, which assumes that the material properties of the overhang, beam 1 a beam 2 are different. Here for the simplicity reason, we assume that these three different parts are made of a same material, i.e., $E = E_1 = E_2$ and $\rho = \rho_1 = \rho_2$, which is a common scenario of many resonator applications [15–18, 38].

Firstly, we compute a special case by setting $b = 2b_1 = 2b_2, h = h_1 = h_2, \Delta_1 = \Delta_2 = 0$ and $\xi_2 = 1$. The above parameters indicate that beam 1 and beam 2 are identical. When the overhang length is $\xi_o = 0$, physically there are two separate beams which vibrate independently. When the overhang length is $\xi_o = 1$, the two beams merge into one. Because it is customary to present the square root of the (dimensionless) eigenfrequency [46], the variations of the first ten $\beta_n$s ($\beta_n = \sqrt{\omega_n}, n = 1$ to 10) as the functions of $\xi_o$ are presented in figure 2. The eigenfrequency square roots of a uniform beam ($f_i$s) are also presented for comparison. For the convenience of statement, we call $\beta_n$ and $f_i$ eigenfrequency hereafter. In figure 2, there are only five eigenfrequencies ($f_i$s, $i = 1$ to 5) whose value is less than 16 and the values of these first five eigenfrequencies ($f_i$s) [46] are presented in table 1. In comparison, in the same range there are ten eigenfrequencies in the overhanged structure. Because the overhang couples the two beams, there are newly emerging eigenfrequencies of $\beta_{2i}$s with even subscript numbers and marked as dashed lines in figure 2. At $\xi_o = 0$, there is no overhang and the two beams are thus uncoupled. The beams are independent and they show the characteristics of a uniform beam, i.e.,

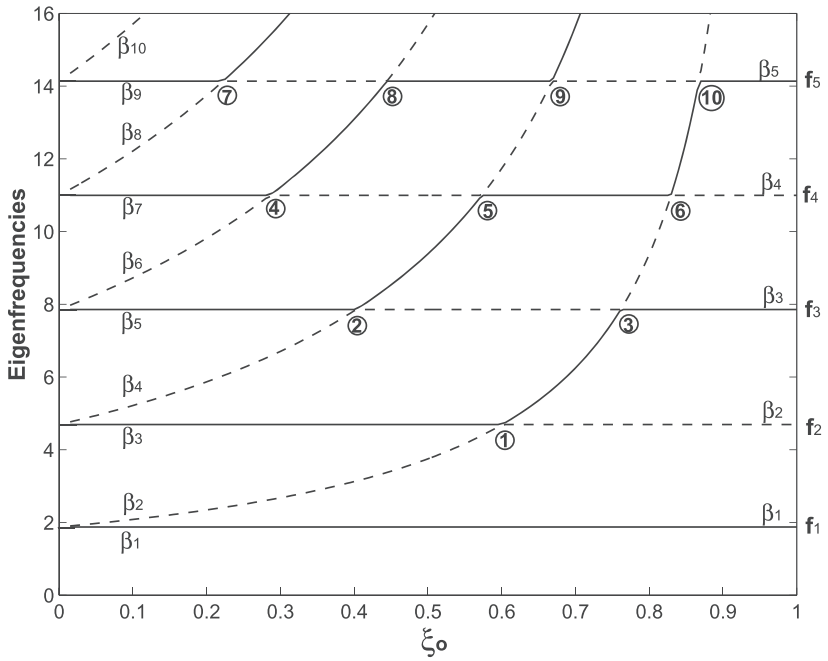


**Figure 2.** The first ten eigenfrequencies ($\beta_n, n = 1$ to 10) as the functions of the overhang length ($\xi_o$) for two identical beams, i.e., $L_1 = L_2, m_1 = m_2$ and $E_1I_1 = E_2I_2$. The dimensions of the overhang are set as $b = 2b_1 = 2b_2$ and $h = h_1 = h_2$; the corresponding dimensionless parameters are $\alpha = \gamma = 2, \kappa = \kappa_2 = 1, \Delta_1 = \Delta_2 = 0$ and $\xi_2 = 1$, respectively. Here $f_i$s ($i = 1$ to 5) are the first five eigenfrequencies of a uniform cantilever beam. The crossing loci are marked by Arabic numbers.

**Table 1.** The first five eigenfrequencies ($f_i$s) of a uniform beam [46] and first ten eigenfrequencies ($\beta_n$s) of the overhanged structure with $\xi_o = 0.1, 0.57, 0.601$ and 0.63. Here $\xi_o = 0.601$ is the $\beta_2/\beta_3$ crossing locus, at which $\beta_2 = \beta_3 = f_2 = 4.694$ and is marked as No. 1 in figure 2.

| Uniform beam | $f_1$ 1.875 | ⋯ | $f_2$ 4.694 | ⋯ | $f_3$ 7.855 | ⋯ | $f_4$ 10.996 | ⋯ | $f_5$ 14.137 | ⋯ |
|---|---|---|---|---|---|---|---|---|---|---|
| Overhanged | $\beta_1$ | $\beta_2$ | $\beta_3$ | $\beta_4$ | $\beta_5$ | $\beta_6$ | $\beta_7$ | $\beta_8$ | $\beta_9$ | $\beta_{10}$ |
| $\xi_o = 0.1$ | 1.875 | 2.083 | 4.694 | 5.216 | 7.855 | 8.728 | 10.996 | 12.217 | 14.137 | 15.708 |
| $\xi_o = 0.57$ | 1.875 | 4.361 | 4.694 | 7.855 | 10.916 | 10.996 | 14.137 | 17.279 | 18.267 | 20.421 |
| $\xi_o = 0.601$ | 1.875 | 4.694 | 4.694 | 7.855 | 10.996 | 11.884 | 14.137 | 17.279 | 19.886 | 20.42 |
| $\xi_o = 0.63$ | 1.875 | 4.694 | 5.068 | 7.855 | 10.996 | 12.686 | 14.137 | 17.279 | 20.422 | 21.229 |

$\beta_{2i-1} = \beta_{2i} = f_i$ at $\xi_o = 0$. At $\xi_o = 0$, the eigenfrequencies of $\beta_{2i-1}$ and $\beta_{2i}$ arise as a pair. As $\xi_o$ increases, $\beta_{2i-1}$ and $\beta_{2i}$ begin to separate: $\beta_{2i-1}$ stays unchanged as $f_i$; while, $\beta_{2i}$ increases rapidly to approach $f_{i+1}$. As the result, the mode associated with $\beta_{2i}$ also experiences the same emerging and then separating process. The similar scenario also occurs in a circular graphene membrane [13] and overhanged beams [26] tuned by an electrostatic force, their resemblance of eigenfrequency emerging and separating is noticed. This new $\beta_{2i}$-mode generating and separating phenomenon is called mode splitting [13, 26]. The emergence of new modes is due to the mixing of modes and mode splitting is equivalent to the transparency [13]. In opto/electromechanics, an electromagnectically induced transparency means that the system is switched from reflecting to transmitting the optical/electromagnetic waves [24, 33, 52].

The variation patterns of the newly emerging eigenfrequencies of $\beta_{2i}$s are also examined. In figure 2, there are ten crossing loci as marked with Arabic numbers. In each crossing locus, $\beta_{2i}$ (dashed line) and $\beta_{2i+1}$ (solid line) experience a rapid approaching-crossing-diverging process. With the increase of the overhang length of $\xi_o$, $\beta_{2i}$ begins to increase rapidly until a crossing locus and then keep constant until a next crossing locus. For example, $\beta_2$ rapidly increases from $\xi_o = 0$ until the crossing locus No. 1 with $\xi_o = 0.601$ and then keeps unchanged as $f_2$ until $\xi = 1$; while, $\beta_4$ increases rapidly until crossing locus No. 2 and keeps constant until crossing locus No. 3, the rapid increase process starts again and stops at crossing locus No. 4, $\beta_4$ finally stays as the constant of $f_4$. For $\beta_{2i-1}$, except $\beta_1$ staying constant, others experience the cycle(s) of staying constant-increasing. For example, $\beta_3$ keeps constant until the crossing locus No. 1 and then rapidly increases until the crossing locus No. 3 and then stays as the constant of $f_3$. In summary, the variation pattern of $\beta_{2i}$ is the cycle(s) of 'rapid increasing-staying constant' and that of $\beta_{2i-1}$ is the cycle(s) of 'staying constant-rapid increasing'. Higher

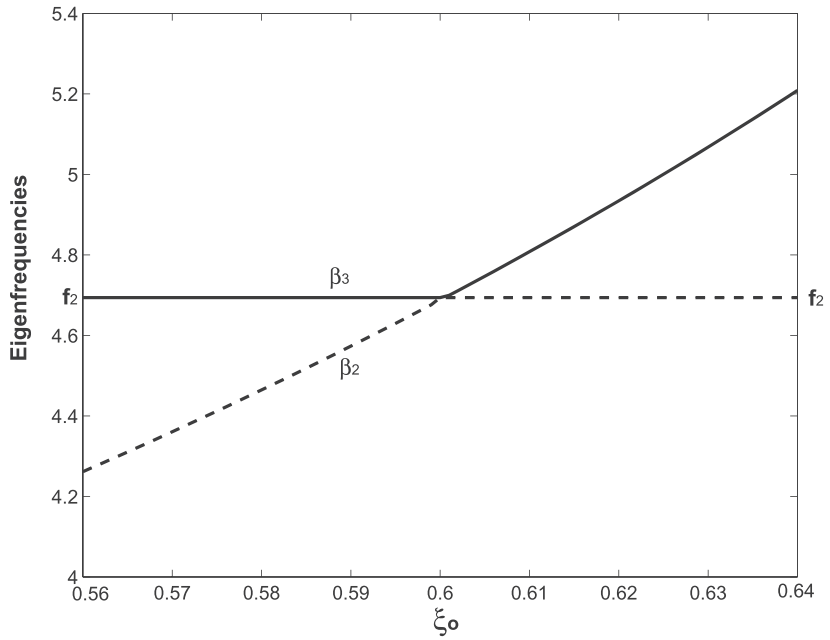


**Figure 3.** A closer look at the crossing of $\beta_3/\beta_2$ around $\xi_o = 0.601$.

eigenfrequency experiences more cycles. In figure 2, the last crossing is No. 10, which is the crossing of $\beta_5/\beta_6$ at $\xi_o = 0.87$. At $\xi_o = 1$, the two overhanged beams now physically become one uniform beam. It is noticed that at $\xi_o = 0$ and $\xi_o = 1$, the system eigenfrequencies are the same as those of a uniform beam ($f_i$s). As the eigenfrequency of a rectangular beam is proportional to $\sqrt{EI/(mL^4)} = \sqrt{Eh^2/(12\rho L^4)}$ [46], the beam width has no impact on the eigenfrequency of a uniform beam. Therefore, the two separate beams with the half width at $\xi_o = 0$ share the same eigenfrequencies of the one beam at $\xi_o = 1$. In figure 2, a clear pattern also arises: when two adjacent eigenfrequencies cross, the other two adjacent eigenfrequencies are separated with the largest distance. For example, at the crossing locus No. 1, $\beta_2$ and $\beta_3$ are closest, while $\beta_2$ and $\beta_1$ are apart with the largest distance. Physically, the closely-spaced $\beta_2$ and $\beta_3$ indicates a weak physical coupling as discussed in equation (1). While, the well-separated $\beta_2$ and $\beta_1$ indicates a strong physical coupling [39] and thus a weak mode coupling [37]. Therefore, both the weak and strong physical couplings with a given overhang length can be achieved by simply exciting two different sets of modes.

Figure 3 presents a closer look at the crossing locus No. 1, which is the $\beta_2/\beta_3$ crossing at $\xi_o = 0.601$. Ten $\beta_n$ values before, at and after the crossing with $\xi_o = 0.57$, 0.601 and 0.63 are also presented in table 1. The crossing pattern is the combined patterns of the $\beta_{2i-1}$ and $\beta_{2i}$ variations as discussed above: Before $\xi_o = 0.601$, $\beta_2$ rapidly increases and $\beta_3$ keeps constant; after $\xi_o = 0.601$, things are reversed: $\beta_2$ keeps constant as $f_2$ and $\beta_3$ rapidly increases. Because it is noted that sometimes it is very hard to distinguish crossing and veering [7, 10, 11], it is worth discussing why the two eigenfrequencies here cross rather than veer. In figures 2 and 3, the special case of two identical beams is handled. As analyzed above, the eigenfrequencies of a uniform beam is independent on its width. Therefore, with any given overhang length ($\xi_o$), there must be an $f_i$ eigenfrequency present all the time in the system. In figure 3, $\beta_3$ initially stays constant as $\beta_3 = f_2$ and $\beta_2$ increases rapidly, they must cross to make $\beta_2 = f_2$ though the two beams are coupled. Physically, the eigenfrequency crossing means the generation of degenerate modes [6] and coupling may not necessarily prevent crossing from occurring. A similar scenario is encountered in a braced beam: when the brace of a translational spring is placed at a beam center, the two eigenvalues (buckling loads or eigenfrequencies) cross [8]. Because the center is a node for some modes, the presence of a spring does not change the system stiffness for those corresponding modes. Furthermore, here the behavior of $\beta_2$ rapid increasing before crossing locus and then keeping constant afterwards, is similar to the 'ideal stiffness' case [8, 9], in which any further increase of the stiffness of a translational bracing spring does not raise the critical buckling load/eigenfrequency and the structure is said to be 'fully braced' [8]. One reason to closely examine this special case of two identical beams is due to the discovery of intrinsic localized mode (ILM) by Sievers and Takeno in 1988 [53]. Unlike the aforementioned defect-induced localization [1], ILM exists in a perfect crystal, which is due to the anharmonicity of lattice [53]. The ILM is also found both in the microscopic system of overhanged microcantilever arrays [54] and in the macroscopic systems of a coupled pendulum array [55] and an electrical transmission line [56]. The so-called mono-element [54] is such case that the two cantilevers, which form a unit in the overhanged microcantilever arrays, are identical. Analogously speaking,

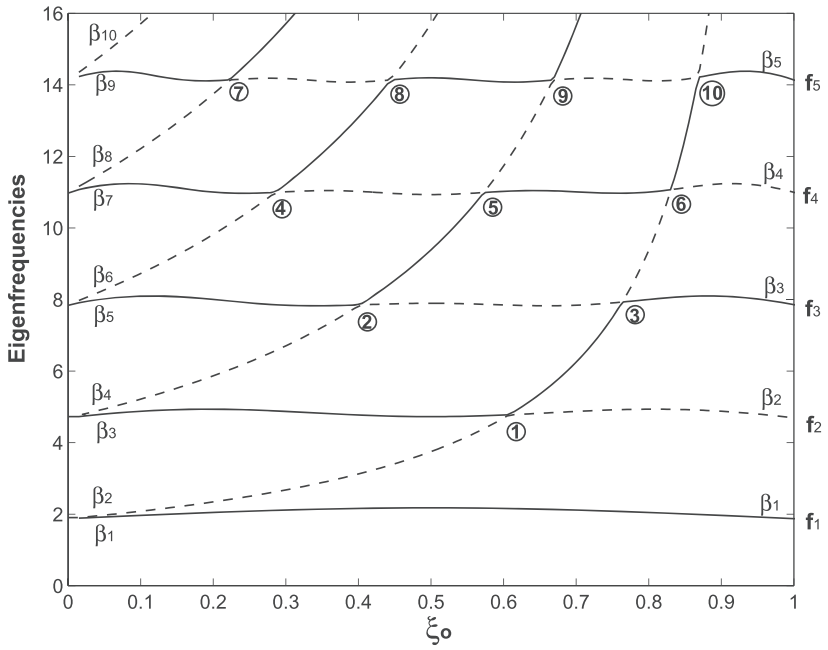


**Figure 4.** The first ten eigenfrequencies as the functions of the overhang length ($\xi_o$) for two identical beams. The dimensions of the overhang are set as $b = 4b_1 = 4b_2$ and $h = h_1 = h_2$. Consequently, the corresponding dimensionless parameters now become $\alpha = \gamma = 4, \kappa = \kappa_2 = 1, \Delta_1 = \Delta_2 = 0$ and $\xi_2 = 1$, respectively.

there is no 'defect' in this two-identical-beam case and it still demonstrates the rapid approaching-diverging behavior of eigenfrequencies, which signals the localization [7].

Compared with the structure in figure 2, the overhang width in figure 4 is doubled as $b = 4b_1 = 4b_2$ and the other parameters are the same as those in figure 2. Again, the first ten eigenfrequencies ($\beta_n$s, $n = 1$ to 10) as the functions of the overhang length $\xi_o$ are plotted. A significant difference between the eigenfrequency variations in figures 2 and 4 is that the horizontal straight lines in figure 2 now become 'wavy' ones in figure 4. Again, $\xi_o = 0$ is the scenario of two separate beams vibrating independently and that $\xi_o = 1$ is the scenario of one beam;both scenarios share the same eigenfrequencies of a uniform beam because, as discussed before, the beam width has no impact on the eigenfrequency of a uniform beam. However, the variation of $\xi_o$ causes the variations of the effective mass and stiffness of the overhanged structure as a whole. Furthermore, $\xi_o$ has different impact on the effective mass and stiffness of different mode shape, which is responsible for the different 'waviness' of different mode. A similar scenario also occurs in a step-like cantilever beam [42]. The ten crossing loci are marked by Arabic numbers and compared with the corresponding crossing locus in figure 2, there is a slight position shift of the crossing locus. For example, the crossing locus No. 1 shifts from $\xi_o = 0.605$ in figure 2 to $\xi_o = 0.625$ in figure 4. In figure 5, the width of the overhang keeps the same as $b = 4b_1 = 4b_2$ of that in figure 4, but the thickness now becomes as $h = 1.6h_1 = 1.6h_2$. Now the variations of eigenfrequencies become more 'wavy'. As discussed above, the eigenfrequencies of a uniform beam are proportional to $\sqrt{Eh^2/(12\rho L^4)}$. As a result, $\beta_{2i-1}$ at $\xi_o = 1$ is larger than $f_i$ because of the increase of thickness. Ten crossing loci are also marked with the Arabic numbers and again, this thickness variation also causes the shifts of the crossing loci.

In figures 2, 4 and 5, the two beams are identical and the impact of the overhang variations on the eigenfrequencies is studied. Now let us examine how a difference, or say, a disorder between the two beams impacts the eigenfrequencies, which is the so-called di-element case [54]. In figures 6 to 12, the dimensions of the overhang are fixed as: $b = 4b_1 = 4b_2$ and $h = 1.6h_1 = 1.6h_2$. In figure 6, the impact of the difference between the two beam lengths on the eigenfrequencies is studied. The parameters of $\xi_o = 0.271$ and $\Delta_1 = \Delta_2 = 0$ are set and fixed. Here $\xi_o = 0.271$ is the crossing locus No. 7 of $\beta_8/\beta_9$ in figure 5 (with $\xi_2 = 1$). The first ten eigenfrequencies as the functions of $\xi_2$ are plotted in figure 6. As defined in equation (7), $\xi_2$ is the dimensionless length of beam 2 and that of beam 1 is always fixed as 1. The general tendency of these ten eigenfrequencies is to decrease with the increase of $\xi_2$ though some eigenfrequencies keep unchanged in certain ranges. The explanation is simple: Shorter beam is stiffer. With a length difference between the two beams, veerings now arise. In figure 6, there are three veering loci and one crossing locus. These three veering loci are at $\xi_2 = 0.585, 0.79$ and 1.21, which are marked by Roman numbers of I, II and IV, respectively. I is the veering locus of $\beta_6$ and $\beta_7$; II is the veering locus of $\beta_7$ and $\beta_8$; IV is the veering locus of $\beta_9$ and $\beta_{10}$. At these three veering loci, all these three pairs of the two adjacent eigenfrequencies rapidly approach and bounce off from the value of

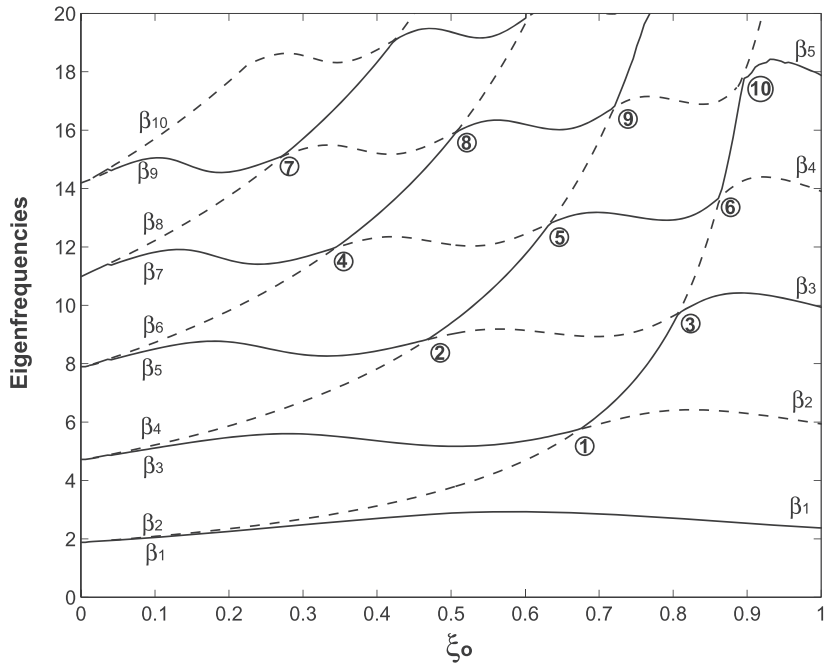


**Figure 5.** The first ten eigenfrequencies as the functions of the overhang length ($\xi_o$) for two identical beams. The dimensions of the overhang are set as $b = 4b_1 = 4b_2$ and $h = 1.6h_1 = 1.6h_2$. Consequently, the corresponding dimensionless parameters now become $\alpha = 6.4, \gamma = 16.384, \kappa = \kappa_2 = 1, \Delta_1 = \Delta_2 = 0$ and $\xi_2 = 1$, respectively.

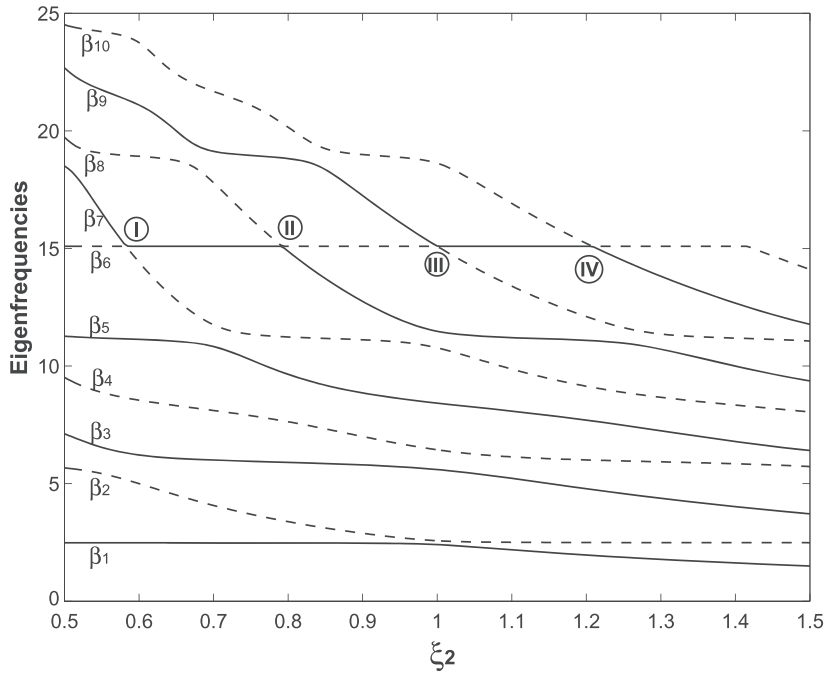


**Figure 6.** The first ten eigenfrequencies as the functions of the beam 2 length ($\xi_2$). The overhang length is $\xi_o = 0.271$.

15.083, which is reason why these four loci are aligned horizontally. III is with $\xi_2 = 1$, i.e., the case of two identical beams. Therefore, III in figure 6 is the $\beta_8/\beta_9$ crossing locus of No. 7 in figure 5.

In figure 7, the overhang length is slightly changed from $\xi_o = 0.271$ to $\xi_o = 0.3$ to see how the crossing/veering loci of I , II, III and IV evolve. There are two outstanding differences occurring. One is that III becomes a veering locus. As seen in figure 5, there is only one $\beta_8/\beta_9$ crossing locus at $\xi_o = 0.271$. As the overhang length is shifted to $\xi_o = 0.3$, the gap between $\beta_8$ and $\beta_9$ enlarges and therefore, there is no crossing locus any more. The other is that the gap between two adjacent eigenfrequencies, i.e., the veering neck [21] or veering width [35], enlarges significantly at each veering locus. Figure 8 presents a comparison and closer look at the veering locus I

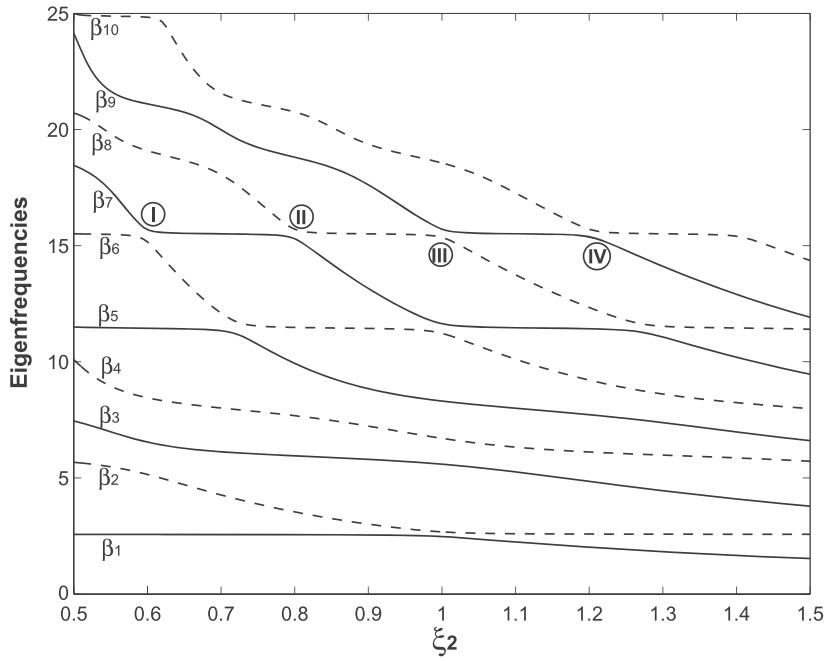


**Figure 7.** The first ten eigenfrequencies as the functions of the beam 2 length ($\xi_2$). The overhang length is $\xi_o = 0.3$.

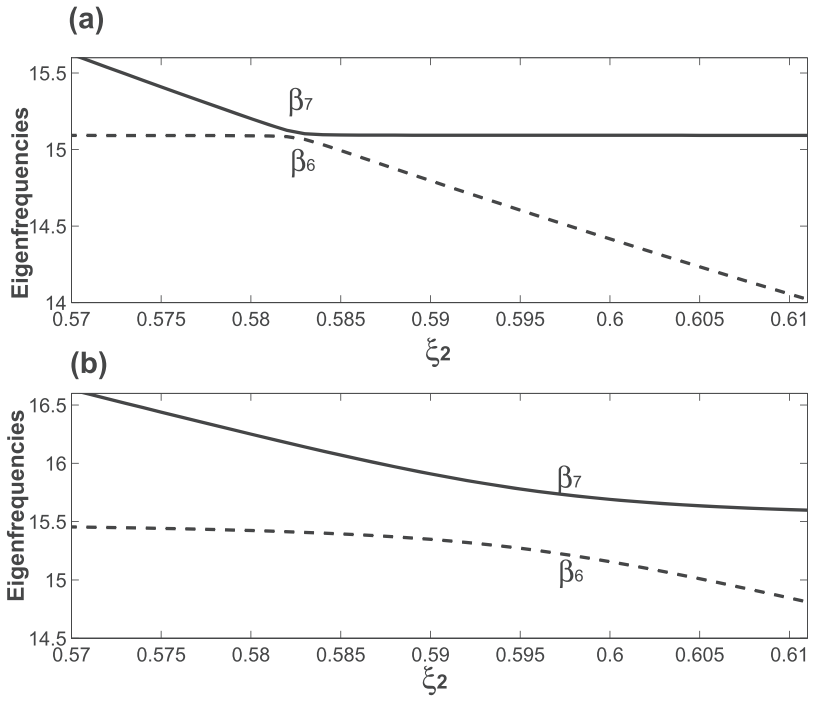


**Figure 8.** A closer look at the veerings of $\beta_6/\beta_7$ with (a) $\xi_o = 0.271$ in figure 6 marked as I and (b) $\xi_o = 0.3$ in figure 7 also marked as I.

in figures 6 and 7. In figure 8(a), $\xi_o = 0.271$ and the veering occurs around $\xi_2 = 0.583$ with the veering neck of $\beta_7 - \beta_6 = 0.036$. In comparison, $\xi_o = 0.3$ in figure 8(b) and the veering occurs around $\xi_2 = 0.597$ with a much larger veering neck of $\beta_7 - \beta_6 = 0.509$. The most outstanding characteristics of veering is that the two eigenfrequencies rapidly approach each other and then bounce off, but they do not cross. Here for the disordered system with two beams of different lengths, the veering mechanism is coupling [2, 6, 10, 11]. The coupling induced by an overhang generates a new mode ($\beta_6$), which approaches rapidly towards a higher mode ($\beta_7$). At the same time, the coupling prevents two eigenfrequencies to cross. The eigenfrequency loci veering as presented in figure 8 can be understood like this: the variation of overhang length brings the two

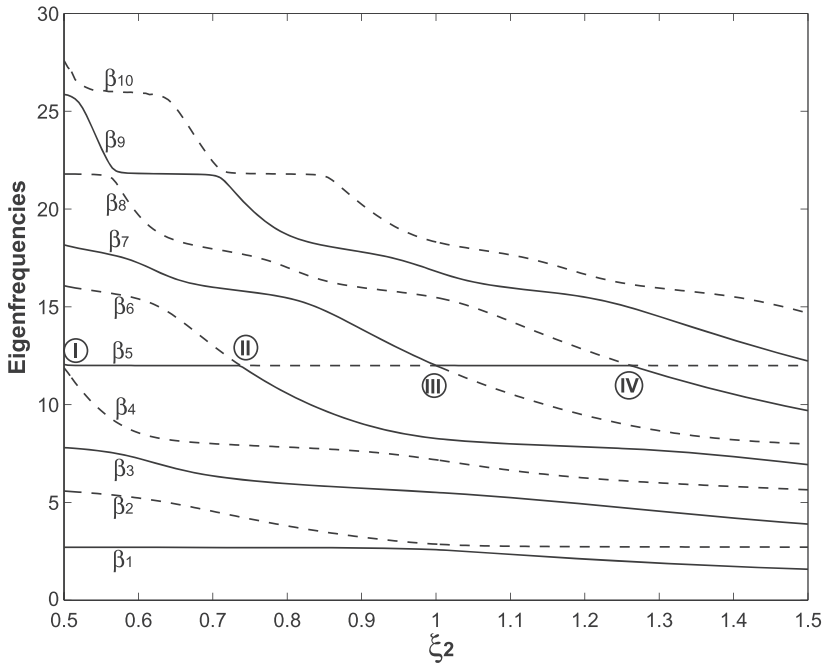


**Figure 9.** The first ten eigenfrequencies as the functions of the beam 2 length ($\xi_2$). The overhang length is $\xi_o = 0.346$.

eigenfrequencies closer; while, the coupling results in a mutual repulsion to push the two eigenfrequencies away from each other [21].

As more veering loci are revealed by varying $\xi_2$ for the fixed overhang length of $\xi_o = 0.271$, we may need to check one more case with a different $\xi_o$ to see if the same pattern holds. In figure 9, $\xi_o$ is changed as $\xi_o = 0.346$, which corresponds to the crossing locus No. 4 (with $\xi_2 = 1$) in figure 5. The first ten eigenfrequencies are plotted as the functions of $\xi_2$. Similar to figure 7, there are three veering loci marked by Roman numbers of I, II and IV, which are at $\xi_2 = 0.5, 0.735$ and 1.26, respectively. Clearly, III with $\xi_2 = 1$ in figure 9 is the crossing locus No. 4 in figure 5. In comparison with those in figure 6, I in figure 9 now is the veering locus of $\beta_4$ and $\beta_5$; II is the veering locus of $\beta_5$ and $\beta_6$; IV is the veering locus of $\beta_7$ and $\beta_8$; III is the crossing locus of $\beta_6$ and $\beta_7$. In conjunction with figures 6, 7 and 9, it is concluded that $\xi_o$ is the paramount parameter of determining the veering loci. The overhang length of $\xi_o$ determines the eigenfrequency value(s) of veering loci. The model of two identical beams can effectively find the eigenfrequency value of a crossing locus together with a corresponding $\xi_o$. In reality, the two beam cannot be identical due to the fabrication errors [54] and these crossing loci thus *de facto* correspond to the veering loci with the smallest veering necks. Furthermore, as shown above, once this $\xi_o$ is found, several more veering loci can be found by varying a beam length.

Besides $\xi_o$ and $\xi_2$, other parameters such as $\Delta_1$ and $\Delta_2$ also have their impacts. In figures 10–12, $\xi_o$ and $\xi_2$ are fixed as $\xi_o = 0.346$ and $\xi_2 = 1$ to study the effects of $\Delta_1$ and $\Delta_2$. In figure 10, the effect of $\Delta_1$ is firstly studied by setting $\Delta_2 = 0$. The first ten eigenfrequencies as the functions of $\Delta_1$ are plotted. As $\Delta_1$ varies from $-0.1$ to 0.1, all ten eigenfrequencies monotonically decrease. The mechanism responsible for this monotonic decrease is simple: as defined in equation (9), $\Delta_1$ is the difference of mass per unit length between beam 2 and 1; larger $\Delta_1$ means more mass for the system, which leads to smaller eigenfrequencies. In the range of $\Delta_1 \in [-0.1, 0.1]$, there is only one crossing locus of $\beta_6$ and $\beta_7$ at $\Delta_1 = 0$, which corresponds to the locus No. 4 in figure 5 or the locus III in figure 9. We can certainly extend the variation range of $\Delta_1$ to see if there are additional crossing or veering loci. However, this variation of $\Delta_1 \in [-0.1, 0.1]$ is actually a huge variation range in the practical applications of many sensitive mass resonator [15, 57]. By setting $\Delta_1 = 0$, the effect of $\Delta_2$ is studied by plotting the first ten eigenfrequencies as the functions of $\Delta_2$ in figure 11. Now all ten eigenfrequencies increase monotonically with $\Delta_2$. As defined in equation (9), $\Delta_2$ is the difference of bending stiffness between beam 2 and 1; larger $\Delta_2$ means a larger stiffness for the whole system, which leads to larger eigenfrequencies. Again, there is only one crossing locus $\beta_6$ and $\beta_7$ at $\Delta_2 = 0$, which, again, is the locus No. 4 in figure 5 or the locus III in figure 9. Once again, the overhang length is the dominant parameter; the parameters of $\Delta_1$ and $\Delta_2$, as seen in figures 10 and 11, serve the tuning function for $\beta_6$ and $\beta_7$.

Figure 12 plots the variations of $\beta_6$ and $\beta_7$ as the functions of $\Delta_1$ and $\Delta_2$. In the studies of eigenvalue veerings, when there is only one varying parameter, the eigenvalue variation is a curve and the corresponding veering problem is thus called curve veering [8]; when there are two varying parameters, the eigenvalue variation

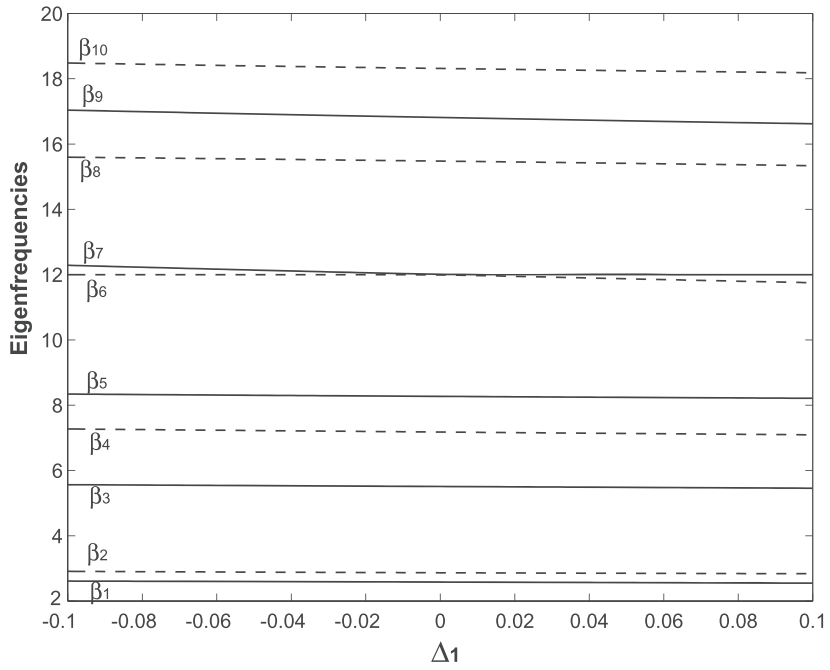


**Figure 10.** The first ten eigenfrequencies as the functions of $\Delta_1$ with $\xi_o = 0.346$, $\xi_2 = 1$ and $\Delta_2 = 0$.

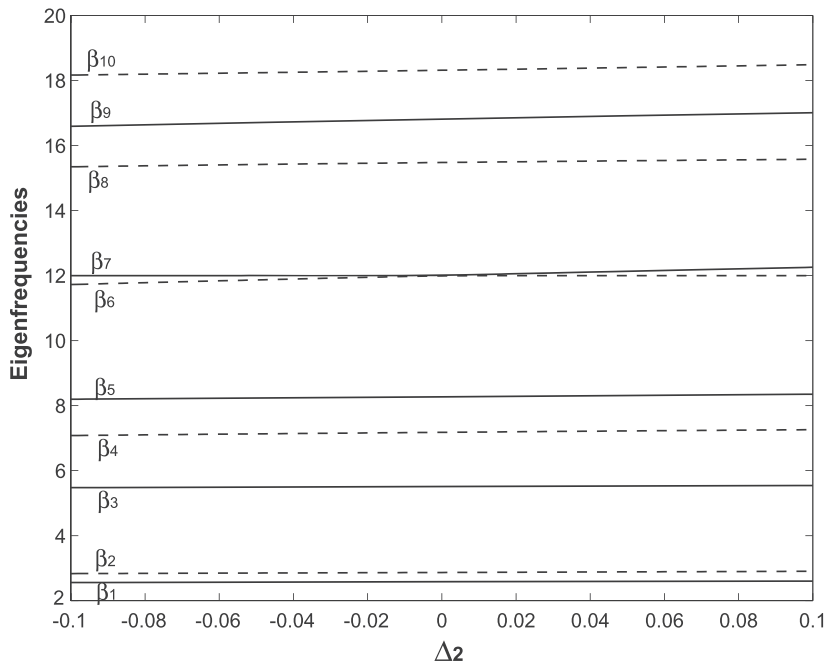


**Figure 11.** The first ten eigenfrequencies as the functions of $\Delta_2$ with $\xi_o = 0.346$, $\xi_2 = 1$ and $\Delta_1 = 0$.

becomes a surface and the name of surface veering is thus given [8]. Similarly, the surface crossing is presented in figure 12. The crossing loci are marked as a dashed line, which is (approximately) a straight line. The explanation for this straight line of crossing loci can be found in equations (11) and (13). The major influence of $\Delta_1$ and $\Delta_2$ on the eigenfrequencies is embodied in the parameter $\kappa_2$ in equation (13) and definition of $\kappa_2$ is given in equation (11) as $\kappa_2 = \sqrt[4]{(1+\Delta_1)/(1+\Delta_2)}$. Therefore, when $\Delta_1$ and $\Delta_2$ vary with a same quantity, which is a straight line, $\kappa_2$ does not change and the crossing loci are thus along this straight line of $\kappa_2 = 1$. Besides $\kappa_2$, $\Delta_2$ also has its influence on the eigenfrequencies through the boundary conditions as seen in the last two equations of equation (12). While, such influence is rather small as $\Delta_2$ varies in the range of $[-0.1, 0.1]$. As the result, the crossing loci are (approximately) a straight line as seen in figure 12.

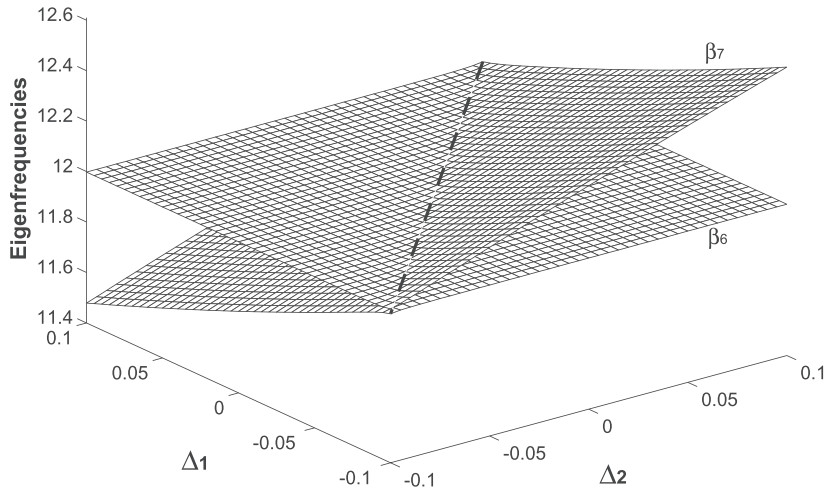


**Figure 12.** The eigenfrequencies of $\beta_6$ and $\beta_7$ as the functions of $\Delta_1$ and $\Delta_1$ with $\xi_o = 0.346$ and $\xi_2 = 1$. The dashed line indicates the crossing loci.

Finally, the limitations of the model need to be addressed. The first is the aforementioned thick beam issue, which lowers the eigenfrequencies of the overhang portion and the veering width can thus vary when $\xi_o$ is small. The second is that no damping is included in the model and damping also lowers the eigenfrequencies. The main reason for no damping is that the damping mechanisms in a microstructure still remain unclear [58]. While, damping is a measured quantity in a real application, which can be simply used as an input. For each mode, its corresponding (dimensional) damping coefficient ($C_i$) is easily obtained by measuring the bandwidth of its frequency response curve [59]. The governing equations of equation (5) are divided into three parts due to the discontinuity of stiffness and mass. By following the approach presented in [60], it is not hard to prove that the operator of equation (5) is self-adjoint and therefore, the orthogonality of the modes holds. With the orthogonality property, the ith eigenfrequency of the damped overhanged structure ($\omega_i^d$) can be easily obtained as: $\omega_i^d = \omega_i\sqrt{1-2\zeta_i^2}$ [59]. Here $\zeta_i = C_i/(2\omega_i)$ and $\omega_i$ is the ith eigenfrequency of the corresponding undamped overhanged structure. This dimensional eigenfrequency is given as $\omega_i = \beta_i^2\sqrt{E_1I_1/(m_1L_1^4)}$ and $\beta_i$s here are those dimensionless results presented in this study. The third is that the uncertainties of the structure dimensions and material properties are not considered. Due to the fabrication tolerance and material variations or defects, the mass (distribution) and stiffness of a microstructure may not be accurately characterized [15, 16, 54]. The solution is to find the effective mass and stiffness by matching the (measured) resonant frequencies or (static) deflections [40], which requires to solve an inverse problem [41, 45]. A more delicate alternative is to use the software/algorithm which can determine those uncertain parameters by quantifying their influence on the outputs [61].

## 4. Conclusions

A continuum model on the overhanged two-cantilever structure, which can be easily extended to an array with multiple cantilevers, is proposed. Unlike a discrete model which only describes two-mode interaction, this continuum model includes the interactions of all modes. The eigenvalue formulation leads to a direct computation on the system eigenfrequencies without any discretization procedure. With this continuum model and a direct computation method, the eigenfrequency loci crossing and veering are presented by simply computing the eigenfrequencies as the functions of the overhang length/thickness and differences of the beam length, stiffness and mass. The overhang couples the two cantilevers, which leads to the mode splitting and then crossing or veering. The mode splitting, which generates a new mode, results from the mixing of two adjacent modes of a beam. With the increase of the overhang length, the rapid eigenfrequency increase of this new mode results in its separation from that of the lower mode, which then leads to its crossing or veering with that of the higher mode. When two beams are identical, crossing occurs with the presence of the overhang coupling effect. When a disorder such as the length, mass or stiffness difference between two beams is introduced, veering occurs due to the coupling mechanism. The overhang length is the most important parameter determining the veering loci; the length difference of the two beams can produce more veering loci. By presenting the

eigenfrequency spectra, a more comprehensive study is provided, which can be useful in the optimum design of the overhanged structures. In the structure of two overhanged cantilevers, the veering indicates the strong mode coupling. The veering locus of two adjacent eigenfrequencies also corresponds to that of two other adjacent eigenfrequencies with the largest separation. Physically, this means that the weak and strong physical couplings can be easily alternated by exciting two different modes, which may hold some potential applications for mass sensing or opto/electromechanics.

## Acknowledgments

This work was jointly supported by the National Natural Science Foundation of China (NSFC, Grant Nos.11772335, 51861145314 and 11872363), the Chinese Academy of Sciences (CAS) Key Research Program of Frontier Sciences (Grant No. QYZDJ-SSW-JSC019), the CAS Strategic Priority Research Program (Grant Nos. XDB22020201 and XDB22040401) and the Russian Foundation for Basic Research, project No. 18-51-80008 (BRICS).22.

## Appendix

The definitions of $b_{31}, b_{32}, b_{41}, b_{42}$ and $c_{31}, c_{32}, c_{41}, c_{42}$

$$b_{31} = \cos(\beta)\cosh(\beta) - \sin(\beta)\sinh(\beta), \quad b_{32} = -\sin(\beta)\cosh(\beta) - \cos(\beta)\sinh(\beta),$$
$$b_{41} = \sin(\beta)\cosh(\beta) - \cos(\beta)\sinh(\beta), \quad b_{42} = \sin(\beta)\sinh(\beta) + \cos(\beta)\cosh(\beta),$$
$$c_{31} = \cos(\kappa_2\beta\xi_2)\cosh(\kappa_2\beta\xi_2) - \sin(\kappa_2\beta\xi_2)\sinh(\kappa_2\beta\xi_2),$$
$$c_{32} = -\sin(\kappa_2\beta\xi_2)\cosh(\kappa_2\beta\xi_2) - \cos(\kappa_2\beta\xi_2)\sinh(\kappa_2\beta\xi_2),$$
$$c_{41} = \sin(\kappa_2\beta\xi_2)\cosh(\kappa_2\beta\xi_2) - \cos(\kappa_2\beta\xi_2)\sinh(\kappa_2\beta\xi_2),$$
$$c_{42} = \sin(\kappa_2\beta\xi_2)\sinh(\kappa_2\beta\xi_2) + \cos(\kappa_2\beta\xi_2)\cosh(\kappa_2\beta\xi_2).$$

The definitions of matrix elements of **K** in equation (14)

$$k_{11} = \sin(\kappa\beta\xi_o) - \sinh(\kappa\beta\xi_o), \quad k_{12} = \cos(\kappa\beta\xi_o) - \cosh(\kappa\beta\xi_o),$$
$$k_{13} = -\sin(\beta\xi_o) - b_{31}\sinh(\beta\xi_o) - b_{41}\cosh(\beta\xi_o), \quad k_{14} = -\cos(\beta\xi_o) - b_{32}\sinh(\beta\xi_o) - b_{42}\cosh(\beta\xi_o),$$
$$k_{21} = \kappa[\cos(\kappa\beta\xi_o) - \cosh(\kappa\beta\xi_o)], \quad k_{22} = -\kappa[\sin(\kappa\beta\xi_o) + \sinh(\kappa\beta\xi_o)],$$
$$k_{23} = -\cos(\beta\xi_o) - b_{31}\cosh(\beta\xi_o) - b_{41}\sinh(\beta\xi_o), \quad k_{24} = \sin(\beta\xi_o) - b_{32}\cosh(\beta\xi_o) - b_{42}\sinh(\beta\xi_o),$$
$$k_{31} = k_{11}, \quad k_{32} = k_{12},$$
$$k_{35} = -\sin(\kappa_2\beta\xi_o) - c_{31}\sinh(\kappa_2\beta\xi_o) - c_{41}\cosh(\kappa_2\beta\xi_o),$$
$$k_{36} = -\cos(\kappa_2\beta\xi_o) - c_{32}\sinh(\kappa_2\beta\xi_o) - c_{42}\cosh(\kappa_2\beta\xi_o),$$
$$k_{41} = k_{21}, \quad k_{42} = k_{22},$$
$$k_{45} = -\kappa_2[\cos(\beta\xi_o) + b_{31}\cosh(\kappa_2\beta\xi_o) + c_{41}\sinh(\kappa_2\beta\xi_o)],$$
$$k_{46} = \kappa_2[\sin(\beta\xi_o) - c_{32}\cosh(\kappa_2\beta\xi_o) - c_{42}\sinh(\kappa_2\beta\xi_o)],$$
$$k_{51} = -\gamma\kappa^2[\sin(\kappa\beta\xi_o) + \sinh(\kappa\beta\xi_o)], \quad k_{52} = -\gamma\kappa^2[\cos(\kappa\beta\xi_o) + \cosh(\kappa\beta\xi_o)],$$
$$k_{53} = \sin(\beta\xi_o) - b_{31}\sinh(\beta\xi_o) - b_{41}\cosh(\beta\xi_o), \quad k_{54} = \cos(\beta\xi_o) - b_{32}\sinh(\beta\xi_o) - b_{42}\cosh(\beta\xi_o),$$
$$k_{55} = -(1+\Delta_2)\kappa_2^2[-\sin(\kappa_2\beta\xi_o) + c_{31}\sinh(\kappa_2\beta\xi_o) + c_{41}\cosh(\kappa_2\beta\xi_o)],$$
$$k_{56} = -(1+\Delta_2)\kappa_2^2[-\cos(\kappa_2\beta\xi_o) + c_{32}\sinh(\kappa_2\beta\xi_o) + c_{42}\cosh(\kappa_2\beta\xi_o)],$$
$$k_{61} = -\gamma\kappa^3[\cos(\kappa\beta\xi_o) + \cosh(\kappa\beta\xi_o)], \quad k_{62} = \gamma\kappa^3[\sin(\kappa\beta\xi_o) - \sinh(\kappa\beta\xi_o)],$$
$$k_{63} = \cos(\beta\xi_o) - b_{31}\cosh(\beta\xi_o) - b_{41}\sinh(\beta\xi_o), \quad k_{64} = -\sin(\beta\xi_o) - b_{32}\cosh(\beta\xi_o) - b_{42}\sinh(\beta\xi_o),$$
$$k_{65} = -(1+\Delta_2)\kappa_2^3[-\cos(\kappa_2\beta\xi_o) + c_{31}\cosh(\kappa_2\beta\xi_o) + c_{41}\sinh(\kappa_2\beta\xi_o)],$$
$$k_{66} = -(1+\Delta_2)\kappa_2^3[\sin(\kappa_2\beta\xi_o) + c_{32}\cosh(\kappa_2\beta\xi_o) + c_{42}\sinh(\kappa_2\beta\xi_o)].$$

## ORCID iDs

Yin Zhang https://orcid.org/0000-0001-5334-0605

## References

[1] Anderson P W 1958 *Phys. Rev.* **109** 1492
[2] Hodges C H 1982 *J. Sound Vibr.* **82** 411
[3] Bendiksen O O 1987 *AIAA J.* **25** 1241
[4] Anderson P W 1978 *Rev. Mod. Phys.* **50** 191

[5] Óttarsson G and Pierre C 1996 *J. Sound Vibr.* **197** 589
[6] Hodges C H and Woodhouse J 1983 *J. Acoust. Soc. Am.* **74** 894
[7] Pierre C 1988 *J. Sound Vibr.* **126** 485
[8] Plaut R H, Murphy K D and Virgin L N 1995 *J. Sound Vibr.* **187** 879
[9] Zhang Y, Liu Y, Cheng P and Murphy K D 2011 *Acta Mech. Solida Sin.* **24** 510 (https://sciencedirect.com/journal/acta-mechanica-solida-sinica/vol/24/issue/6)
[10] Leissa A W 1974 *J. Appl. Math. Phys.* **25** 99
[11] Perkins N C and Mote C D 1986 *J. Sound Vibr.* **106** 451
[12] Brown K R, Ospelkaus C, Colomber Y, Wilson A C, Leibfried D and Wineland D J 2011 *Nature* **471** 196
[13] Mathew J P, Patel R N, Borah A, Vijay R and Deshmukh M M 2016 *Nat. Nanotech.* **11** 747
[14] Novotny L 2010 *Am. J. Phys.* **78** 1199
[15] Spletzer M, Raman A, Wu A Q and Xu X 2006 *Appl. Phys. Lett.* **88** 254102
[16] Spletzer A, Raman A, Sumali H and Sullivan J P 2008 *Appl. Phys. Lett.* **92** 114102
[17] DeMartini B E, Rhoads J F, Shaw S W and Turner K L 2007 *Sens. Actuators A: Phys.* **137** 147
[18] DeMartini B E, Rhoads J F, Zielke M Z, Owen K G, Shaw S W and Turner K L 2008 *Appl. Phys. Lett.* **93** 054102
[19] Gil-Santos E, Ramos D, Jana A, Calleja M, Raman A and Tamayo J 2009 *Nano Lett.* **9** 4122
[20] Gil-Santos E, Ramos D, Pini V, Calleja M and Tamayo J 2011 *Appl. Phys. Lett.* **98** 123108
[21] Thiruvenkatanathan P, Woodhouse J, Yan J and Seshia A A 2011 *J. Microelectromechan. Syst.* **20** 157
[22] Thiruvenkatanathan P, Woodhouse J, Yan J and Seshia A A 2011 *J. Appl. Phys.* **109** 104903
[23] Teufel J D, Li D, Allman M, Cicak K, Sirois A, Whittaker J and Simmonds R 2011 *Nature* **471** 204
[24] Chan J, Alegre T, Safavi-Naeini A, Hill J, Krause A, Gröblacher S, Aspelmeyer M and Painter O 2011 *Nature* **478** 89
[25] Mahboob I, Nishiguchi K, Okamoto H and Yamaguchi H 2012 *Nat. Phys.* **8** 387
[26] Okamoto H, Gourgout A, Chang C, Onomitsu K, Mahboob I, Chang E and Yamaguchi H 2013 *Nat. Phys.* **9** 480
[27] Faust T, Rieger J, Seitner M, Krenn P, Kotthaus J and Weig E 2012 *Phys. Rev. Lett.* **109** 037205
[28] Faust T, Krenn P, Manus S, Kotthaus J and Weig E 2012 *Nat. Commun.* **3** 728
[29] Faust T, Rieger J, Seitner M, Kotthaus J and Weig E 2013 *Nat. Phys.* **9** 485
[30] Barton R *et al* 2012 *Nano Lett.* **12** 4681
[31] Shkarin A, Flowers-Jacobs N, Hoch S, Kashkanova A, Deutsch C, Reichel J and Harris H 2014 *Phys. Rev. Lett.* **112** 013602
[32] Aspelmeyer M, Kippenberg T and Marquardt F 2014 *Rev. Mod. Phys.* **86** 1391
[33] Metzger C and Karral K 2004 *Nature* **432** 1002
[34] Gil-Santos E, Ramos D, Martínez J, Fernández-Regúlez M, Garcia R, San Paulo A, Calleja M and Tamayo J 2010 *Nat. Nanotech.* **5** 641
[35] Glean A, Judge J, Vignola J and Ryan T 2015 *J. Appl. Phys.* **117** 054505
[36] Natsiavas S 1993 *J. Sound Vibr.* **165** 137
[37] Eichler A, del Álamo Ruiz M, Plaza J and Bachtold A 2012 *Phys. Rev. Lett.* **109** 025503
[38] Karabalin R B, Cross M C and Roukes M L 2009 *Phys. Rev.* B **79** 165309
[39] Hajhashemi M, Rasouli A and Bahreyni B 2016 *J. Microelectromechan. Syst.* **25** 52
[40] Zhang Y 2011 *J. Vibr. Acoust.* **133** 021006
[41] Choubey B, Anthony C, Saad N, Ward M, Turnbull R and Collins S 2010 *Appl. Phys. Lett.* **97** 133114
[42] Gao F and Zhang Y 2018 *AIP Adv.* **8** 045108
[43] Timoshenko S and Woinowsky-Krieger A 1959 *Theory of Plates and Shells* (New York: McGraw-Hill Book Company, Inc)
[44] Whitney J M 1987 *Structural Analysis of Laminated Anisotropic Plates* (Basel: Technomic Publishing Company, Inc.)
[45] Zhang Y 2017 *Int. J. Mech. Sci.* **128–129** 572
[46] Chang T C and Craig R R 1969 *J. Engr. Mech.* **195** 1027
[47] Press W H, Flannery B P, Teukolsky S A and Vettering W T 1986 *Numerical Recipes* (Cambridge: Cambridge University Press)
[48] Samaniego E, Anitescu C, Goswami C, Nguyen-Thanh V M, Guo H, Hamdia K, Zhuang X and Rabczuk T 2020 *Comput. Methods Appl. Mech. Engrg.* **362** 112790
[49] Guo H, Zhuang X and Rabczuk T 2019 *Comput. Mater. Con.* **59** 433
[50] Rabczuk T, Ren H and Zhuang X 2019 *Comput. Mater. Con.* **59** 31
[51] Anitescu C, Atroshchenko E, Alajlan N and Rabczuk T 2019 *Comput. Mater. Con.* **59** 345
[52] Weis S, Rivière R, Deléglise S, Gavartin E, Arcizet O, Schliesser A and Kippenberg T 2010 *Science* **330** 1520
[53] Sievers A J and S Takeno S 1988 *Phys. Rev. Lett.* **61** 970
[54] Sato M, Hubbard B E and Sievers A J 2006 *Rev. Mod. Phys.* **78** 137
[55] Thakur R B, English L Q and Sievers A J 2008 *J. Phys. D: Appl. Phys.* **41** 015503
[56] Stearrett R and English L Q 2007 *J. Phys. D: Appl. Phys.* **40** 5394
[57] Zhang Y 2014 *Sens. Actuators B: Chem.* **202** 286
[58] Mohanty P, Harrington D A, Ekinci K L, Yang Y T, Murphy M J and Roukes M L 2002 *Phys. Rev.* B **66** 085416
[59] Meirovitch L 2001 *Fundamentals of Vibrations* (New York: McGraw-Hill Companies, Inc.)
[60] Zhang Y and Murphy K D 2007 *Acta Mech. Solida Sin.* **20** 236
[61] Vu-Bac N, Lahmer T, Zhuang X, Nguyen-Thoi T and Rabczuk T 2016 *Adv. Eng. Softw.* **100** 19